1 **Title: Cancer cell-autonomous cGAS-STING response confers drug resistance**

2 **Running title: Cancer cell-autonomous STING activation drives drug resistance**

3 Qian-Ming Lv[1,#], Shi-Yi Wang[1,#], Hui-Min Lei[1,#], Ke-Ren Zhang[1], Ya-Bin Tang[1], Ying

4 Shen[1], Li-Ming Lu[3,*], Hong-Zhuan Chen[2,*], Liang Zhu[1,*]

5 [1]Department of Pharmacology and Chemical Biology, College of Basic Medical

6 Sciences and Respiratory Department, Shanghai Chest Hospital, Shanghai Jiao Tong

7 University School of Medicine, Shanghai 200025, China.

8 [2]Department of Clinical Pharmacy, Institute of Interdisciplinary Integrative Biomedical

9 Research, Shuguang Hospital, Shanghai University of Traditional Chinese Medicine,

10 Shanghai 201203, China.

11 [3]Shanghai Institute of Immunology, College of Basic Medical Sciences & Central

12 laboratory, Shanghai Chest Hospital, Shanghai Jiao Tong University School of

13 Medicine, Shanghai 200025, China.

14 #These authors contributed equally to this work.

15 ***Corresponding author:**

16 Liang Zhu, Department of Pharmacology and Chemical Biology, College of Basic

17 Medical Sciences and Respiratory Department, Shanghai Chest Hospital, Shanghai Jiao

18 Tong University School of Medicine, Shanghai 200025, China. Email:

19 jyzhul@shsmu.edu.cn

20 Hong-Zhuan Chen, Department of Clinical Pharmacy, Institute of Interdisciplinary

21 Integrative Biomedical Research, Shuguang Hospital, Shanghai University of

22 Traditional Chinese Medicine, Shanghai 201203, China. Email: yaoli@shsmu.edu.cn

23 Li-Ming Lu, Central laboratory, Shanghai Chest Hospital & Shanghai Institute of

24 Immunology, Shanghai Jiao Tong University School of Medicine, Shanghai 200025,

25 China. Email: lulunew2003@163.com

26

Conflicts of interest

28   The authors declare that they have no competing interests.

Abstract

30   As an evolutionarily conserved DNA-sensing machinery in innate immunity, the cGAS-
31   STING pathway has been reported to play an important role in immune surveillance
32   and tumor suppression. Recent evidence suggests an intriguing tumor- and metastasis-
33   promoting effect of this signaling pathway, either in a cancer cell-autonomous or a
34   cancer cell-nonautonomous, bystander cell-mediated manner. Here, we show a new
35   face of cGAS-STING signaling whose activation in a cancer-cell-autonomous response
36   manner confers drug resistance. Targeted or conventional chemotherapy drug treatment
37   induced cancer cell cytosolic DNA accumulation and triggered subsequent cGAS-
38   STING signaling activation in cancer cell lines and the human cell-derived xenograft
39   tumors. This activation promoted an acquisition and maintenance of drug resistance
40   which was prevented and overcome in vitro and in vivo by blockade of STING
41   signaling. This finding highlights a new face of cGAS-STING signaling and an ability
42   of cancer cells to hijack the evolutionarily conserved inflammatory signaling to
43   counteract drug stress and warrants a caution in combining STING agonist with
44   targeted or conventional chemotherapy drug treatment, a strategy prevailing in current
45   clinical trials.

Statement of significance

47   cGAS-STING signaling has long been recognized as playing a key role in triggering
48   antitumor immunity. We reveal a new face of cGAS-STING signaling and an ability of
49   cancer cells autonomously to hijack the evolutionarily conserved inflammatory
50   signaling to counteract drug stress.

Introduction

51

52 STING (stimulator of interferon genes) serves as a linchpin in the cytosolic DNA-

53 sensing pathway. Activated by cyclic GMP-AMP (cGAMP) that is produced by cyclic

54 GMP-AMP synthase (cGAS) sensing cytosolic double-stranded DNA (dsDNA),

55 STING boosts downstream inflammatory signaling (1,2). Discovered primarily as an

56 important machinery in innate immunity and host defense against microbial pathogens,

57 cGAS-STING has been extendedly depicted as playing a key role in triggering

58 antitumor immunity (1,2).

59 The putative tumor-suppressive effect of STING motivates the research and

60 development of STING agonists for cancer immunotherapy. However, the limited

61 efficacy of these STING agonist in clinical trials warrants a more comprehensive

62 understanding of cGAS-STING characteristics (1,2). Recently, evidence suggests an

63 intriguing cancer and metastasis-promoting effect of cancer cell-intrinsic cGAS-

64 cGAMP-STING activation, either in a cancer cell-autonomous response manner (3,4)

65 or in a cancer cell-nonautonomous, bystander cell-mediated manner (5), indicating the

66 many faces of cGAS-STING signaling in cancer biology other than triggering

67 antitumor immunity which has received more attention (1,2,6,7).

68 Resistance is one of the biggest challenges for cancer treatment (8). Based on our in

69 vitro and in vivo cancer targeted therapy resistance models (9-11) , we repeatedly and

70 curiously noticed that an activated rather than suppressed status was achieved in cGAS-

71 STING signaling when these cancer cells acquired resistance to therapeutic drugs. We

72 hypothesized that the cells that can upregulate cGAS-STING signaling would acquire

73 the ability to cope with drug stress and evolve drug resistance.

74 Herein, we show that a cancer-cell-autonomous response of the cell-intrinsic cGAS-

75 STING activation triggered by targeted or chemotherapy drugs confers drug resistance.

76 This finding highlights a novel face of cGAS-STING signaling and a skill of cancer

77 cells hijacking the evolutionarily conserved inflammatory signaling to counteract drug

78 stress and warrant a caution in combining a STING agonist with anti-cancer drugs, a

79   prevailing strategy in current clinical trial designs.

80   **Results**

81   **Hyperactivation of cGAS-STING signaling in drug-resistant tumor and tumor**
82   **cells**

83   Transcriptomic analysis of the differentially expressed genes between the various lines
84   of EGFR TKI-resistant cells (Supplementary Fig. S1A, top panel) versus their isogenic
85   parental sensitive cells demonstrated an enrichment for cytosolic DNA sensing pathway
86   (Supplementary Fig. S1B, top panel). The enrichment was recapitulated in
87   chemotherapy drug cisplatin-resistant cells (Supplementary Fig. S1B, bottom panel)
88   and in vivo drug-resistant models (Supplementary Fig. S1A, bottom panel) where the
89   erlotinib treatment-relapsed tumors showed a hyperactivation of cytosolic DNA sensing
90   signature compared with the sensitive tumors (Fig. 1A). Likewise, cGAS-STING
91   downstream target genes were upregulated in resistant cells (Fig. 1B, Supplementary
92   Fig. S1C).

93   Consistently, the resistant cells showed an intracellular accumulation of cytosolic DNA
94   (Fig. 1C and D; Supplementary Fig. S1D), the endogenous cGAS agonist, and cGAMP
95   (Fig. 1E), the cGAS-generated second messenger. Accordingly, the active form of
96   cGAS and STING (cGAS dimers and STING dimers, respectively) (Fig. 1F) and the
97   activated STING, phosphorylated STING (p-STING) (Fig. 1G) were accordingly
98   upregulated in resistant cells. The activation of cGAS-STING was reconfirmed by RT-
99   qPCR analysis showing the upregulation of signaling downstream gene expression
100   (Supplemental Fig. S1E and S1F, red bar vs. grey bar), which depended on STING
101   (Supplemental Fig. S1F).

102   **Addiction of resistant cells to STING pathway**

103   These STING-activated, drug-resistant cells were more sensitive to STING knockdown
104   or inhibition compared with their parental cells, assayed by the cell growth monitoring

4

105   (Fig. 1H; Supplemental Fig. S2A and S2B) and viability (Fig. 1I; Supplemental Fig.

106   S2C) analyses. Meanwhile, resistant cells demonstrated enhanced colony formation

107   ability (Fig. 1J; Supplemental Fig. S2D) and epithelial-mesenchymal transition (EMT)

108   properties including EMT gene enrichment (Supplemental Fig. S2E), epithelial marker

109   and mesenchymal markers change (Supplemental Fig. S2F), morphologic transition

110   (Supplemental Fig. S2G, OR vs. P), and migration ability (Fig. 1K; Supplemental Fig.

111   S2H and S2I). These enhanced drug resistance properties were abrogated by STING

112   knockdown (Fig. 1K, L; Supplemental Fig. S2G-S2I).

Resistance to targeted and conventional chemotherapy drugs depends on STING
activation

115   Knockdown of STING, either transiently by small interfering RNA (siRNA;

116   Supplementary Fig. S3A) or constantly by short hairpin RNA (shRNA; Supplementary

117   Fig. S3B and S3C), resensitized EGFR TKI-resistant cells to the corresponding TKI

118   osimertinib (Fig. 1M; Supplementary Fig. S3D and S3E), erlotinib (Supplementary Fig.

119   S3F), and gefitinib (Supplementary Fig. S3G). The resensitization was recapitulated by

120   STING selective inhibitor H151 (Fig. 1N). Moreover, STING knockdown (Fig. 1O;

121   Supplementary Fig. S3H-S3J) or inhibition (Fig. 1P) sensitized H460 large cell lung

122   carcinoma cells, MCF-7 breast cancer cells, SW620 colon cancer cells, C33A cervical

123   cancer cells, and the KRAS-G12S mutated, non-targetable A549 lung cancer cells to

124   chemotherapy drug cisplatin, indicating that cancer cells refractory to conventional

125   chemotherapy drugs depend on STING activation.

Targeted or conventional chemotherapy drug treatment triggers cGAS-STING
pathway activation

128   We then investigated how the cGAS-STING signaling was activated. Treatment with

129   the targeted therapy drug osimertinib induced an intracellular accumulation of cytosolic

130   dsDNA in sensitive cells (Fig. 2A), coincided with an induction of DNA damage as

131   shown by an upregulation of the DNA double-strand break marker γ-H2AX (Fig. 2B).

132   Consistently, accumulation of intracellular cGAMP (Fig. 2C) and upregulation of cGAS

133   dimers and STING dimers (Fig. 2D) were demonstrated in these cells treated with

134   osimertinib.

135   Consequently, cGAS-STING signaling was triggered, evidenced by a time-dependent

136   increase of activated form of pathway regulators and effectors p-STING, p-TBK1, p-

137   IRF3, and p-p65 after osimertinib treatment (Fig. 2E). The activation sustained

138   throughout the whole process of resistance emergence and maintenance in in vitro and

139   in vivo models (Fig. 2E and F). This drug stress-induced STING downstream signaling

140   activation was not confined to targeted therapies, as evidenced by an activation of

141   STING signaling in breast cancer MCF-7 cells underwent cisplatin treatment (Fig. 2G),

142   extending to chemotherapy situations. The activation was abrogated by cGAS

143   suppression (Fig. 2H), indicating its dependence on cGAS.

STING activation is sufficient for resistance induction

145   Exogenous supplement of cGAMP, the endogenous STING agonist, induced the

146   otherwise sensitive cells resistant to TKIs (Supplementary Fig. S3K). This resistance-

147   induction effect of STING activation was recapitulated by more cell membrane-

148   permeable STING agonist ADU-S100 (Fig. 2I) treatment in targeted therapy (Fig. 2J;

149   Supplementary Fig. S3L) and in chemotherapy situations (Fig. 2K). Moreover, ADU-

150   100 administration was sufficient to induce EMT, a key property for resistance, as

151   demonstrated by marker change (E-cad downregulation and Vim upregulation) (Fig. 2L)

152   and migration enhancement (Fig. 2M).

STING confers resistance via activation of TBK1-IRF3/p65 NF-κB signaling

154   Transcriptomic analysis showed inflammatory properties in EGFR TKI-resistant

155   tumors (Fig. 3A; Supplementary Fig. S4A) and cells (Supplementary Fig. S4B).

156   Consistently, analysis of public clinical data recorded in The Cancer Genome Atlas

6

157   (TCGA) database showed that in targeted and chemotherapy drug-treated lung cancer

158   patients, inflammatory response properties were enriched in tumors with EMT features

159   (Supplementary Fig. S4C), a well-known drug resistance mechanism (12). Western blot

160   analysis demonstrated in resistant cells an upregulation of STING downstream

161   inflammatory signaling factors p-STING, p-IRF3, and p-p65 (Fig. 2E, 2F, and 3B)

162   which depended on STING (Fig. 3C). IRF3 and p65 were important for resistant cell

163   survival (Fig. 3D), growth (Supplementary Fig. S4D), EMT/migration (Fig. 3E and F;

164   Supplementary Fig. S4E and S4F), and insensitivity to TKIs (Fig. 3G and H;

165   Supplementary Fig. S4G-S4L). STING activation depended on IRF3 and p65 for drug

166   resistance induction, as shown by the fact that the STING activation-induced

167   osimertinib resistance was completely abrogated by the combination of IRF3

168   knockdown and p65 knockdown (Fig. 3I).

169   STING instigated IRF3 and p65 signaling via TBK1. Targeted and chemotherapy drugs

170   induced an activation of TBK1 in sensitive cells (Fig. 2E and G) and the activation was

171   maintained in resistance phase (Fig. 2E, 2F, and 3B). Both the TKI-induced activation

172   of TBK1 in sensitive cells (Fig. 3J, left panel) and the constitutive activation of TBK1

173   in resistant cells (Fig. 3J, right panel) were abrogated by STING knockdown. This

174   TBK1 activation controlled downstream IRF3 and p65, evidenced by a nullification of

175   upregulated p-IRF3 and p-65 in resistant cells by TBK1 selective inhibitor amlexanox

176   (Fig. 3K).

177   Then we examined if TBK1 mediated the STING-induced drug resistance and cell

178   EMT/migration enhancement. Genetic knockdown (Supplementary Fig. S5A) or

179   pharmacological inhibition of TBK1 selectively suppressed the resistant cell viability

180   (Fig. 3L; Supplementary Fig. S5B) and EMT/migration properties (Fig. 3M;

181   Supplementary Fig. S5C and 5D) and resensitized these cells to targeted (Fig. 3N and

182   O; Supplementary Fig. S5E) and chemotherapy (Fig.3P; Supplementary Fig. S5F)

183   drugs. Additionally, TBK1 suppression abrogated the STING activation-induced

184   osimertinib resistance (Fig. 3Q; Supplementary Fig. S5G) and migration enhancement

185   (Supplementary Fig. S5H).

186   **Drug resistance acquisition and maintenance in vivo depend on STING activation**

187   STING signaling was triggered and activated by drug treatment and the activation was

188   maintained throughout the whole process of resistance emergence and maintenance

189   (Fig. 2E-G) and this activation was required and sufficient for drug resistance in vitro.

190   We next examined whether the role of STING signaling in drug resistance was

191   recapitulated in vivo in immunodeficient nude mice. HCC827 cell-derived xenograft

192   (CDX) tumors initially responded well to osimertinib with growth delay and volume

193   decrease after osimertinib administration but resistance was acquired after continuous

194   drug treatment as shown by a tumor burden relapse (Fig. 4A). Blockade of STING

195   signaling with amlexanox not only prevented the acquisition of resistance but also

196   resensitized the resistance-acquired tumors to osimertinib (Fig. 4 A, B, and C),

197   indicating that both the resistance acquisition and maintenance depend on STING

198   signaling in vivo. STING signaling blockade with amlexanox did not cause mouse body

199   weight change (Supplementary Fig. S5I).

200   Consistently, analysis of public clinical data recorded in TCGA database showed that

201   in targeted and chemotherapy drug-treated lung cancer patients, cytosolic DNA sensing

202   pathway was enriched in tumors with EMT features (Fig. 4D). Meanwhile, the patients

203   whose tumors expressed higher abundance of STING demonstrated a lower drug

204   response (Fig. 4E) and relapse-free survival (RFS) probability (Fig. 4F). In patients who

205   underwent drug treatment and got DNA damage in tumors, higher expression of STING

206   correlated with lower RFS probability (Fig. 4G). Additionally, lung cancer patients with

207   enhanced cGAS-STING signaling signature demonstrated lower overall survival

208   probability (Supplementary Fig. S5J).

209   The negative effect of STING on drug response was recapitulated in breast (Fig. 4H

210   and I) and ovarian ((Fig. 4J) cancers, where higher expression of STING predicted

211   inferior response to chemotherapies.

Discussion

212

213 Recent progress has uncovered the multifaceted roles of STING signaling in cancer
214 biology, not only triggering anticancer immune response around the tumor but also
215 inducing tumorigenesis and metastasis (1,2).

216 In this study, we find a new face of cGAS-STING signaling whose activation in a
217 cancer-cell-autonomous response manner confers cancer drug resistance, highlighting
218 a potent ability of cancer cells hijacking the evolutionarily conserved inflammatory
219 signaling to copy with drug stress.

220 Anticancer drugs that act primarily through DNA-damaging mechanism, such as
221 etoposide, cisplatin, and PARP inhibitors, have been reported to trigger cytosolic DNA
222 accumulation and cGAS-STING signaling activation (3,13). Besides chemotherapy
223 drugs, the molecularly targeted drug EGFR TKIs, acting primarily not as traditional
224 chemotherapy cytotoxic agents, have been demonstrated in this study, also induced
225 cancer cell cytosolic DNA accumulation and triggered the cell-intrinsic cGAS-
226 cGAMP-STING activation and downstream signaling transduction.

227 STING activation was sufficient and necessary for acquisition and maintenance of the
228 cancer drug resistance. Activation of STING induced drug resistance acquirement,
229 which was abrogated by STING antagonism in vitro; blockade of STING signaling
230 prevented the acquired resistance and the subsequent tumor relapse to therapy in vivo,
231 indicating the importance of STING activation on drug resistance emergence. On the
232 other hand, STING activation also plays important roles in maintenance of the
233 resistance. First, resistant cells exhibited a constitutive hyperactivation of STING
234 signaling which is pivotal for survival and withstanding drug insult demonstrated by
235 the fact that genetic or pharmacological blockade of STING signaling selectively
236 suppressed the resistant cells and resensitized the cells to drug treatment. Second, in
237 vivo, drug-resistant and relapse were overcome by blockade of STING signaling.

238 STING conferred resistance through its TBK1-IRF3/NF-κB downstream signaling.
239 TBK1 stands at the hub of STING signaling and inflammatory responses and is

240 essential to cancer cell survival and growth (14,15). Moreover, recent discoveries have

241 identified TBK1 as a key point and a therapeutic target for cancer drug resistance (16,17)

242 and the activation of TBK1-IRF3 signaling has been reported to protect cells from drug-

243 induced death (18). We found that the STING-conferred drug resistance depended on

244 its downstream p65-relied canonical NF-κB signaling. Effect of canonical NF-κB

245 signaling on drug resistance induction has been reported (19). STING-induced

246 metastasis, in contrast, was mediated by noncanonical NF-κB signaling (4). It is

247 intriguing that cancer metastasis and drug resistance are mediated by divergent

248 pathways of STING downstream signaling, deserving further investigation.

249 Taken together, targeted or conventional chemotherapy drug-induced activation of

250 cGAS-STING in cancer cells confers these cells an ability to withstand the drug

251 challenge in a cancer cell-adapted and autonomous response manner. DNA directly or

252 indirectly damaged by drug pressure leaks into the cytosol. The accumulated cytosolic

253 DNA is intrinsically sensed and responded by cGAS-cGAMP-STING signaling

254 pathway. Cancer cells can take advantage of this pathway via the downstream TBK1-

255 IRF3/NF-κB signaling to counteract drug stress and acquire resistance to these drugs

256 (Fig. 4K).

257 This finding has important implications for a better understanding of cGAS-STING

258 functions and cancer therapies. First, a new face of STING signaling and a novel skill

259 of cancer cells autonomously adapted for counteracting drug stress are uncovered and

260 formally proposed. Second, the cancer-cell-autonomous effects of the cell-intrinsic

261 cGAS-STING activation, other than the modulation of microenvironmental immune

262 cells, are worthy of attention. Third, there are numerous STING agonists being

263 clinically tested, either as a single agent or in combination with targeted or

264 chemotherapy drugs (20), our discovery of STING activation as a drug resistance-

265 inducing mechanism implies a possible explanation, at least partly, for their limited

266 efficacy and warrant a caution in designing these kinds of combination strategies.

267   **Methods**

268   **Cells and Cell Culture**

269   Human lung adenocarcinoma cell lines that harbor EGFR-activating mutations,

270   HCC827 and H1975, were obtained from American Type Culture Collection (ATCC),

271   PC9 from Dr. G.L. Zhuang (China State Key Laboratory of Oncogenes and Related

272   Genes). Human large cell lung cancer cell line H460, human lung adenocarcinoma cell

273   line A549, human cervical cancer cell line C33A, human breast cancer cell line MCF7,

274   and human colorectal cancer cell line SW620 were obtained from Dr. Q. Lu

275   (Department of Pharmacology and Chemical Biology, Shanghai Jiao Tong University

276   School of Medicine). The cells were authenticated by short tandem repeat (STR)

277   analysis. Cell lines which are resistant to erlotinib (HCC827ER), gefitinib

278   (HCC827GR), and osimertinib (HCC827OR and H1975OR1–5) were established,

279   maintained, and authenticated as schematized (Supplementary Fig. 1A) and previously

280   described (9-11). The cells were cultured in RPMI 1640 medium (Gibco, USA)

281   containing 10% FBS, 1% GlutaMAX, and 1% penicillin- streptomycin at 37 °C with

282   5% CO2.

283   **Reagents and antibodies**

284   Erlotinib and gefitinib were purchased from LC Laboratories. Osimertinib, amlexanox,

285   QNZ (EVP4593) were purchased from Selleck Chemicals. ADU-S100 were purchased

286   from MCE. Dimethyl sulfoxide (DMSO) was obtained from Sigma. Antibodies for

287   dsDNA and p-IRF3 were purchased from Abcam; for E-cadherin, vimentin, β-actin,

288   STING, p-STING, TBK1, p-TBK1, p65, p-p65, IRF3 and γH2AX from Cell Signaling

289   Technology; for cGAS from Sigma.

290   **Cell Growth and Viability Assay**

291   Cells were seeded in 96-well plates at a density of 4,000 cells/well. After the cells

292 adhering to the well, corresponding treatment agents were added to the medium. Cell

293 growth was monitored using the IncuCyte ZOOM live cell analysis system (Essen

294 Bioscience). Cell viability was determined using the Cell Counting Kit-8 (CCK-8;

295 Dojindo) assay according to the manufacturer's instructions.

Colony Formation Assay

296

297 Cells were seeded in 6-well plates (1,000 cells/well) for treatments and cultured in

298 complete medium for about 1 week. Fixed with 4% paraformaldehyde for 15 minutes,

299 the cells were stained with 0.01% crystal violet for counting. Individual colonies (>50

300 cells) were counted.

Transwell Migration Assay

301

302 Migration assays were performed by using Transwell chambers (Corning Costar). After

303 the corresponding treatments, the cells (50,000 per chamber) were plated into the upper

304 chambers containing serum-free medium whereas the lower chambers were filled with

305 medium containing 10% FBS. After 24 hours, the cells attached to the underside of the

306 filter were stained with 0.1% crystal violet solution and imaged (Nikon). Then, the

307 stained cells were dissolved with 10% acetic acid (100 μL/chamber), and the optical

308 density (OD) was detected at 600 nm using a microplate reader to quantify the cell

309 migration ability.

Western Blot and Immunofluorescence Analysis

310

311 Western blot and immunofluorescence analyses were performed according to standard

312 protocols. First antibodies are described in Methods or indicated in corresponding

313 figure legends.

Gene knockdown by RNA interference

314

315 For transient knockdown, cells were transfected with small interfering RNAs (siRNAs)

12

316 using Lipofectamine 3000 reagent (Invitrogen, USA) according to the manufacturer's

317 instructions. Target sequences were used as shown in Supplementary Table S1. For

318 constant knockdown, endogenous STING was silenced by using short hairpin RNA

319 (shRNA), with scrambled shRNAs as controls. Shortly, pGIPZ-shSTING expression

320 clones were packaged with pMD2.G and pSPAX2. For transfection, cells were seeded

321 in 6-well plates at density of 200,000/well. Twenty-four hours later, the lentiviral

322 particles were diluted with serum-free medium containing 6 μg/mL polybrene. The

323 sense sequences of shRNAs were shown in Supplementary Table S1.

324 **Liquid Chromatography and Tandem Mass Spectrometry Analysis of cGAMP**

325 Cell samples were analyzed on an Exion® LC-system coupled with a TripleQUAD®

326 6500 plus system (Sciex, Concord, ON, USA). A volume of 5 μL was injected onto a

327 BEH HILIC UPLC column (1.7 μm, 100 × 3 mm; Waters). The column oven was 35 °C.

328 The mobile phase was set as follows: (A) 10 mM ammonium fluoride and 0.1%

329 ammonia in water, (B) pure acetonitrile. The initial condition was 45% A, maintained

330 for 1 min. The mobile phase was ramped to 72% A from 1 min to 7 min, then maintained

331 at 45% A from 7.01 min to 10 min. The flow rate was set to 0.4 ml/min. The mass

332 spectrometer was operated in Electron Spray Ionization (ESI) negative mode with the

333 source temperature 550 °C. Declustering and collision-induced dissociation were

334 achieved with nitrogen gas. The multiple reaction monitoring (MRM) transition,

335 declustering potential (DP) and collision energy for cGAMP measurement were as

336 follows: m/z 673.1 [M-H]- → 344.1, -200 V, -50 eV. The analytic data were processed

337 using AnalystTM 1.7 software and MultiQuantTM 3.0 software (Sciex, Concord, ON,

338 USA).

339 **Animal Study and In Vivo Xenografts Assay**

340 Animal work was evaluated and approved by the Institutional Animal Care and Use

341 Committee (IACUC) of Shanghai Jiao Tong University School of Medicine. In cell-

13

342   derived xenograft (CDX) studies, one hundred microliters of phosphate buffered saline

343   (PBS) containing 5×10^6 cancer cells were subcutaneously injected into the left and

344   right flanks of 4-week-old BALB/c nu/nu athymic mice. Subcutaneous local tumors

345   were measured on length (L) and width (L) by a Vernier caliper every 2-3 days and the

346   volume of tumors were calculated with the formula: $V = LW^2/2$. When tumor volume

347   reached ~ 200 mm^3, mice were randomized into different treatment groups as described

348   in figure legends. Mice were euthanized when the animal experiments reached the end

349   or the tumor volume of the vehicle control group reached 1,500 mm^3.

Combination Effect Analysis

351   Treatment combinations will lead to synergy, antagonism, or additive effect. A

352   calculation of Combination Index (CI) based on Chou Talalay method (21)

353   (Chou06PharmacoRev) was used to evaluated the combination effects. CompuSyn

354   software (CompuSyn Inc. USA) was utilized to analyze the data.

Statistical analysis

356   Quantitative data are presented as mean $\pm$ SEM of at least three independent

357   experiments. Differences were assessed using the two-tailed Student's t test or ANOVA

358   with Bonferroni posttest unless otherwise indicated. $P < 0.05$ was considered

359   statistically significant. *, $P < 0.05$; **, $P < 0.01$. ***, $P < 0.001$; ****, $P < 0.0001$

360   unless otherwise indicated.

Reference

362   1.   Kwon J, Bakhoum SF. The Cytosolic DNA-Sensing cGAS-STING Pathway in

363   Cancer. Cancer Discov **2020**;10(1):26-39 doi 10.1158/2159-8290.CD-19-0761.

364   2.   Vashi N, Bakhoum SF. The Evolution of STING Signaling and Its Involvement

365   in   Cancer.   Trends   Biochem   Sci   **2021**;46(6):446-60   doi

366   10.1016/j.tibs.2020.12.010.

367   3.   Ahn J, Xia T, Konno H, Konno K, Ruiz P, Barber GN. Inflammation-driven
368   carcinogenesis is mediated through STING. Nat Commun **2014**;5:5166 doi
369   10.1038/ncomms6166.

370   4.   Bakhoum SF, Ngo B, Laughney AM, Cavallo JA, Murphy CJ, Ly P*, et al.*
371   Chromosomal instability drives metastasis through a cytosolic DNA response.
372   Nature **2018**;553(7689):467-72 doi 10.1038/nature25432.

373   5.   Chen Q, Boire A, Jin X, Valiente M, Er EE, Lopez-Soto A*, et al.* Carcinoma-
374   astrocyte gap junctions promote brain metastasis by cGAMP transfer. Nature
375   **2016**;533(7604):493-8 doi 10.1038/nature18268.

376   6.   Li J, Bakhoum SF. Expanding the Role of STING in Cellular Homeostasis and
377   Transformation.   Trends   Cancer   **2019**;5(4):195-7   doi
378   10.1016/j.trecan.2019.02.001.

379   7.   Hopfner KP, Hornung V. Molecular mechanisms and cellular functions of
380   cGAS-STING signalling. Nat Rev Mol Cell Biol **2020**;21(9):501-21 doi
381   10.1038/s41580-020-0244-x.

382   8.   Vasan N, Baselga J, Hyman DM. A view on drug resistance in cancer. Nature
383   **2019**;575(7782):299-309 doi 10.1038/s41586-019-1730-1.

384   9.   Ma CS, Lv QM, Zhang KR, Tang YB, Zhang YF, Shen Y*, et al.* NRF2-
385   GPX4/SOD2 axis imparts resistance to EGFR-tyrosine kinase inhibitors in non-
386   small-cell lung cancer cells. Acta Pharmacol Sin **2021**;42(4):613-23 doi
387   10.1038/s41401-020-0443-1.

388   10.   Lei HM, Zhang KR, Wang CH, Wang Y, Zhuang GL, Lu LM*, et al.* Aldehyde
389   dehydrogenase 1A1 confers erlotinib resistance via facilitating the reactive
390   oxygen species-reactive carbonyl species metabolic pathway in lung
391   adenocarcinomas. Theranostics **2019**;9(24):7122-39 doi 10.7150/thno.35729.

392   11.   Zhang KR, Zhang YF, Lei HM, Tang YB, Ma CS, Lv QM*, et al.* Targeting
393   AKR1B1 inhibits glutathione de novo synthesis to overcome acquired
394   resistance to EGFR-targeted therapy in lung cancer. Sci Transl Med

395   **2021**;13(614):eabg6428 doi 10.1126/scitranslmed.abg6428.

396 12. Shibue T, Weinberg RA. EMT, CSCs, and drug resistance: the mechanistic link

397   and clinical implications. Nat Rev Clin Oncol **2017**;14(10):611-29 doi

398   10.1038/nrclinonc.2017.44.

399 13. Dunphy G, Flannery SM, Almine JF, Connolly DJ, Paulus C, Jonsson KL*, et al.*

400   Non-canonical Activation of the DNA Sensing Adaptor STING by ATM and

401   IFI16 Mediates NF-kappaB Signaling after Nuclear DNA Damage. Mol Cell

402   **2018**;71(5):745-60 e5 doi 10.1016/j.molcel.2018.07.034.

403 14. Zhu L, Li Y, Xie X, Zhou X, Gu M, Jie Z*, et al.* TBKBP1 and TBK1 form a

404   growth   factor   signalling   axis   mediating   immunosuppression   and

405   tumourigenesis. Nat Cell Biol **2019**;21(12):1604-14 doi 10.1038/s41556-019-

406   0429-8.

407 15. Hu L, Xie H, Liu X, Potjewyd F, James LI, Wilkerson EM*, et al.* TBK1 is a

408   Synthetic Lethal Target in Cancer with VHL Loss. Cancer Discov **2019** doi

409   10.1158/2159-8290.CD-19-0837.

410 16. Eskiocak B, McMillan EA, Mendiratta S, Kollipara RK, Zhang H, Humphries

411   CG*, et al.* Biomarker Accessible and Chemically Addressable Mechanistic

412   Subtypes   of   BRAF   Melanoma.   Cancer   Discov   **2017**;7(8):832-51   doi

413   10.1158/2159-8290.CD-16-0955.

414 17. Kitajima S, Asahina H, Chen T, Guo S, Quiceno LG, Cavanaugh JD*, et al.*

415   Overcoming   Resistance   to   Dual   Innate   Immune   and   MEK   Inhibition

416   Downstream   of   KRAS.   Cancer   Cell   **2018**;34(3):439-52   e6   doi

417   10.1016/j.ccell.2018.08.009.

418 18. Gong K, Guo G, Panchani N, Bender ME, Gerber DE, Minna JD*, et al.* EGFR

419   inhibition triggers an adaptive response by co-opting antiviral signaling

420   pathways in lung cancer. Nat Cancer **2020**;1(4):394-409 doi 10.1038/s43018-

421   020-0048-0.

422 19. Taniguchi K, Karin M. NF-kappaB, inflammation, immunity and cancer:

423   coming of age. Nat Rev Immunol **2018**;18(5):309-24 doi 10.1038/nri.2017.142.

424   20.   Vanpouille-Box C, Hoffmann JA, Galluzzi L. Pharmacological modulation of

425   nucleic acid sensors - therapeutic potential and persisting obstacles. Nat Rev

426   Drug Discov **2019**;18(11):845-67 doi 10.1038/s41573-019-0043-2.

427   21.   Chou TC. Theoretical basis, experimental design, and computerized simulation

428   of synergism and antagonism in drug combination studies. Pharmacol Rev

429   **2006**;58(3):621-81 doi 10.1124/pr.58.3.10.

430

431

Acknowledgements

Author contributions:

Q.-M.L. and H.-M.L. established in vitro and in vivo experiment conditions. Q.-M.L. performed analyses for cell growth, viability, western blot, and in vivo response under drug treatment. Q.-M.L. performed analyses for TCGA, RNA-seq, and omics data mining. S.-Y.W. and K.-R.Z. cultured cells, performed analyses for cell colony formation and apoptosis. Y.S. provided study materials and contributed to manuscript writing and revision. L.-Q.M., S.-Y.W., and H.-M.L. designed the study, analyzed the data, and contributed to manuscript writing and revision. L.-M.L and H.-Z.C interpreted data, acquired financial support, and contributed to manuscript writing and review. H.-Z.C contributed to oversight and leadership responsibility for the research and approved the manuscript. L.Z designed study conception and experiments, assembled and interpreted data, wrote the manuscript, and approved the manuscript.

Figure legends

Figure 1. Drug-resistant cancer cells demonstrate and depend on an activated cGAS-STING signaling

(A) Gene set enrichment analysis (GSEA) of RNA-seq data indicates a hyperactivation of cytosolic DNA sensing pathway in erlotinib treatment-relapsed tumors (n=5) compared with the sensitive tumors (n=6). The schematic diagram of the establishment of the in vivo models is shown in Supplementary Fig. S1A.

(B) Heatmap shows expression difference of cGAS-STING signaling downstream genes between HCC827 TKI-resistant (ER and GR) and parental (Par) cells assayed by

457   RNA-seq analysis. ER and GR represent erlotinib and gefitinib resistance, respectively.

458   (C) Double-strand DNA (dsDNA) accumulation in the cytoplasm of HCC827OR

459   resistant versus parental (P) cells assayed by anti-dsDNA antibody (1:50, Abcam)-

460   based immunofluorescence staining analysis. Scale bar: 50 μm.

461   (D) Extranuclear DNA accumulation in HCC827 resistant (ER, GR, OR) versus

462   parental (P) cells assayed by quantification of relative extranuclear DAPI fluorescence

463   intensity.

464   (E) Accumulation of intracellular cGAMP, the cGAS-generated second messenger, in

465   HCC827OR versus parental cells assayed by LC-MS/MS analysis.

466   (F) Western blot analysis of cGAS and STING proteins in HCC827OR versus parental

467   cells.

468   (G) Upregulation of p-STING in resistant cells, assayed by western blot analysis.

469   (H) Effect of STING siRNA treatment (20 nM, 48 h) on cell growth in H1975OR versus

470   parental cells. The cell growth was monitored and quantified using IncuCyte ZOOM

471   system every 4 h. Mock siRNA at 20 nM as control.

472   (I) Effect of STING knockdown (20 nM siRNA, 72 h) on cell viability in TKI-resistant

473   cells versus parental cells. STING siRNA versus mock siRNA: ns, not significant; *, p

474   < 0.05; **, p < 0.01; ***, p < 0.001; ****, p < 0.0001.

475   (J) Effect of STING knockdown (10 nM siRNA, 48 h) on colony formation for 7 days

476   in HCC827 resistant (ER, GR, OR) cells versus parental cells. Cells at a density of

477   1,000/well in 6-well plate were seeded at the beginning of the assay. Resistant versus

478   parental: #, p < 0.05; ##, p < 0.01; ### p < 0.001; ####, p < 0.0001. STING siRNA

479   versus mock siRNA: *, p < 0.05; **, p < 0.01; ***, p < 0.001; ****, p < 0.0001.

480   (K) Effect of STING siRNA treatment on cell migration in HCC827 resistant (ER, GR,

481   OR) cells versus parental cells. After 20 nM STING or mock siRNA treatment for 48

482   h, the cells were trypsinized, resuspended, and adjusted to 50,000/well in transwell for

483   incubation of 24 h for cell migration. Resistant versus parental: ##, p < 0.01. STING

484   siRNA versus mock siRNA: *, p < 0.05; **, p < 0.01. Representative images are

19

485   demonstrated in Supplementary Fig. S2H.

486   (L) Western blot analysis of epithelial marker E-cadherin (E-cad) and mesenchymal

487   marker vimentin (vim). C, control, M, mock.

488   (M and N) Effect of STING knockdown (M, 10 nM siRNA for 72 h) or inhibition (N,

489   10 μM H151 for 72 h) on TKI sensitivity in TKI-resistant cells. Combination index was

490   calculated according to Chou Talalay method as described in Methods.

491   (O and P) Effect of STING knockdown (O, 20 nM siRNA for 72 h) or inhibition (P, 10

492   μM H151 for 72 h) on cisplatin sensitivity in H460 human large cell lung carcinoma

493   cells and C33A human cervical cancer cells.

494

Figure 2. Drug treatment-triggered activation of cGAS-STING signaling is sufficient for resistance induction

497   (A) Immunofluorescence staining analysis of dsDNA accumulation in the cytoplasm of

498   HCC827 cells exposed to TKI acute treatment (1 μM osimertinib for 2 h). Scale bar: 50

499   μm.

500   (B) Western blot analysis of DNA damage marker γH2AX in PC9 cells exposed to 1

501   μM osimertinib as indicated period.

502   (C) LC-MS/MS analysis of intracellular cGAMP in HCC827 cells exposed to 1 μM

503   osimertinib for 72 h.

504   (D) Western blot analysis of cGAS dimer and STING dimer in HCC827 cells exposed

505   to 1 μM osimertinib as indicated period.

506   (E) Western blot analysis of cGAS-STING signaling activation markers p-STING, p-

507   TBK1, p-IRF3, and p-p65 in the process of resistance emergence and maintenance

508   (sensitive, tolerant, and resistant/relapsed phases) in in vitro and in vivo models.

509   HCC827 cells in the sensitive phase were exposed to 1 μM osimertinib as indicated

510   period. OT200 and OT500 are HCC827-derived cell lines that are tolerant to 200 and

511   500 nM osimertinib, respectively. OR1000 is the HCC827-derived cell line that is

512   resistant to 1,000 nM osimertinib. CDXOR is the HCC827CDX tumor in BALB/c

513   nu/nu athymic mice relapsed to osimertinib (2 mg/kg, p.o., q.d.) treatment.

514   (F) Western blot analysis of cGAS-STING signaling activation markers p-STING, p-

515   TBK1, p-IRF3, and p-p65 in PC9 tolerant and resistant model cell lines to osimertinib.

516   OT200 and OT500 are PC9-derived cell lines that are tolerant to 200 and 500 nM

517   osimertinib, respectively. OR1000 is the PC9-derived cell line that is resistant to 1000

518   nM osimertinib.

519   (G) Western blot analysis of cGAS-STING signaling activation markers in MCF-7 cells

520   exposed to 100 μM cisplatin as indicated periods.

521   (H) Effect of cGAS knockdown on osimertinib-induced STING signaling activation.

522   After incubated with 20 nM cGAS or mock siRNA for 24 h, the cells were further

523   exposed to 1 μM osimertinib for 24 h.

524   (I) Concentration-dependent effect of STING agonist ADU-S100 on osimertinib

525   sensitivity in HCC827 and H1975 cells. After incubated with indicated concentrations

526   of ADU-S100 for 24 h. The cells were exposed to 1 μM osimertinib for 48 h.

527   (J and K) Effect of ADU-S100 on TKIs (J) and cisplatin (K) sensitivity. After incubated

528   with 10 μM ADU-S100 for 24 h, the cells were exposed further to indicated

529   concentrations of individual TKIs or 33 μM cisplatin for 48 h.

530   (L) Effect of ADU-S100 (10 μM for 24 h) on STING signaling and EMT markers in

531   HCC827 cells.

532   (M) Effect of ADU-S100 on H1975 and HCC827 cell migration. After 10 μM ADU-

533   S100 treatment for 24 h, the cells were trypsinized, resuspended, and adjusted to

534   50,000/well in transwell for incubation of 24 h for cell migration. *, $p < 0.05$; **, $p <$

535   0.01.

536

537   **Figure 3. STING confers resistance via activation of TBK1-IRF3/NF-κB signaling**

538   (A) GSEA of RNA-seq data indicates an inflammatory hallmark in erlotinib treatment-

539   relapsed tumors (n=5) compared with the sensitive tumors (n=6).

540   (B) Western blot analysis of STING downstream inflammatory signaling markers p-

541   TBK1, p-IRF3, and p-p65 in resistant (ER, GR, OR) versus parental (P) cells.

542   (C) Effect of STING knockdown (20 nM siRNA) on STING downstream inflammatory

543   signaling in HCC827OR cells.

544   (D) Selective effect of IRF suppression (20 nM siRNA for 72 h) on resistant cell

545   viability.

546   (E) Selective effect of IRF suppression (20 nM siRNA for 48 h) on enhanced migration

547   in HCC827ER, GR, and OR resistant cells (representative images in Supplementary

548   Fig. S4E). After IRF siRNA or mock siRNA treatment for 48 h, the cells were

549   trypsinized, resuspended, and adjusted to 50,000/well in transwell for incubation of 24

550   h for cell migration. Resistant versus parental: #, $p < 0.05$; ##, $p < 0.01$; ###, $p < 0.001$.

551   siIRF3 versus mock: *, $p < 0.05$; **, $p < 0.01$; ***, $p < 0.001$.

552   (F) Effect of IRF3 suppression (20 nM siRNA for 48 h) on resistant cell EMT markers.

553   (G and H) Effect of suppression of IRF3 (G, 10 nM siRNA for 72 h) or p65 (H, 5 μM

554   QNZ for 72 h) on osimertinib concentration-cell viability inhibition response curves in

555   HCC827OR cells.

556   (I) Effect of a combination of IRF knockdown and p65 knockdown on the STING

557   activation-induced osimertinib resistance. The cells were incubated with 10 μM ADU-

558   S100 for 24 h, and exposed further to 20 nM IRF siRNA, 20 nM p65 siRNA, 1 μM

559   osimertinib alone, or in combination as indicated for 48 h.

560   (J) Effect of STING knockdown on osimertinib acute treatment-induced TBK1

561   activation in HCC827 parental cells (left panel) and on the constitutively activated

562   TBK1 in HCC827OR cells (right panel). Parental cells were treated with 20 nM STING

563   siRNA for 48 h and then exposed to 1 μM osimertinib for 2 h; OR cells were treated

564   with 20 nM STING siRNA for 72 h.

565   (K) Effect of TBK1 suppression (amlexanox for 48 h) on cGAS-STING signaling and

566   EMT markers in HCC827OR cells.

567   (L and M) Effect of TBK1 suppression (20 nM siRNA) on resistant cell viability (L)

568   and enhanced migration (M, representative images in Supplementary Fig. S5C).

569   siRNAs were used for 72 h in viability assay and for 48 h in the migration assay.

570   (N and O) Effect of TBK1 knockdown (N, 10 nM siRNA, 72 h) or inhibition (O,

571   amlexanox, 72 h) on osimertinib sensitivity in HCC827OR and H1975OR resistant

572   cells.

573   (P) Effect of TBK1 suppression (amlexanox, 72 h) on cisplatin sensitivity in MCF-7

574   and A549 cells.

575   (Q) Effect of TBK1 suppression (20 μM amlexanox, ALX) on STING activation (10

576   μM ADU-S100)-induced osimertinib resistance. After incubated with ADU-S100 for

577   24 h, the cells were further exposed to osimertinib with or without ALX for 48 h.

578

579   **Figure 4. Drug resistance acquisition and maintenance in vivo depend on STING**

580   **signaling**

581   (A and B) Effect of STING signaling blockade with amlexanox on prevention and

582   reversal of osimertinib resistance in HCC827CDX tumors. Shown are tumor growth

583   over time (A) and tumor weights at day 30 and day 66 (B). R-Osi represents continued

584   osimertinib single agent treatment for relapsed tumors; R-Combo represents

585   osimertinib + amlexanox combination treatment for relapsed tumors; Combo represents

586   the osimertinib + amlexanox combination treatment throughout the whole experiment).

587   Flank subcutaneously implanted, HCC827 cell-derived xenograft tumors (2 tumors per

588   mouse), when reached ~ 200 mm^3, were randomized into groups, at day 13: Vehicle

589   control (n=5), Amlexanox (n=5), Osimertinib (n=10), and Combo (combination of

590   amlexanox and osimertinib) (n=5). At day 46 post tumor inoculation, 7 mice in

591   osimertinib group relapsed and were randomly regrouped into Osimertinib

592   (continuation) arm (n=3) and Amlexanox + Osimertinib arm (n=4). STING signaling

593   pathway inhibitor amlexanox and EGFR TKI osimertinib were administered (p.o., q.d.)

594 as 50 mg/kg and 2 mg/kg, respectively.

595 (C) Representative images of hematoxylin and eosin (H&E) staining for pathological

596 analysis and immunohistochemistry (IHC) staining of the cell proliferation marker Ki-

597 67 for in situ analysis of cell proliferation. Scale bar: 100 μm.

598 (D) GSEA of RNA-seq data indicates an increased activation of cytosolic DNA sensing

599 pathway in tumors with EMT versus tumors with non-EMT signature in lung cancer

600 patients that have undergone targeted or chemotherapy drug treatment (Six patients

601 have tumors with prototypical EMT signature [Vimentin expression abundance ranks

602 top 10% and E-cadherin ranks bottom 10% in total tumors] and 5 with prototypical non-

603 EMT signature [Vimentin ranks bottom 10% and E-cadherin ranks top 10%]. Two

604 hundred eighty-eight patients who had drug treatment information in TCGA data were

605 analyzed. Vimentin and E-cadherin are mesenchymal and epithelial maker, respectively.

606 (E) Response profiles of lung cancer patients underwent EGFR TKI (n=24) or

607 chemotherapy (n=206) treatment. CR, complete response. PR, partial response. SD,

608 stable disease. PD, progressive disease.

609 (F and G) Kaplan-Meier analysis of relapsed shows that lower free survival (RFS)

610 probability was correlated with higher tumor STING expression in lung cancer patients

611 underwent chemotherapy (F) and in lung cancer patients who underwent targeted and

612 chemotherapy drug treatment as well as got DNA damage in their tumors (G).

613 In E, F, G, data were retrieved from TCGA data set (http://cancergenome.nih.gov/). The

614 patients were stratified according to high versus low expression (cutoff: median) of

615 STING mRNA abundance within their tumors.

616 (H-J) Box-plots and ROC (receiver operating characteristic) curves of predictive effect

617 of STING on chemotherapy response defined as RFS in ovarian cancer (H),

618 pathological response (I) and RFS (J) in breast cancer. The analyses were performed

619 according to the ROC Plotter tool (http://www.rocplot.org/).

620 (K) Schematic demonstration of the drug resistance conferred by cancer cell-

621 autonomous cGAS-STING response to drug treatment stress. Created with
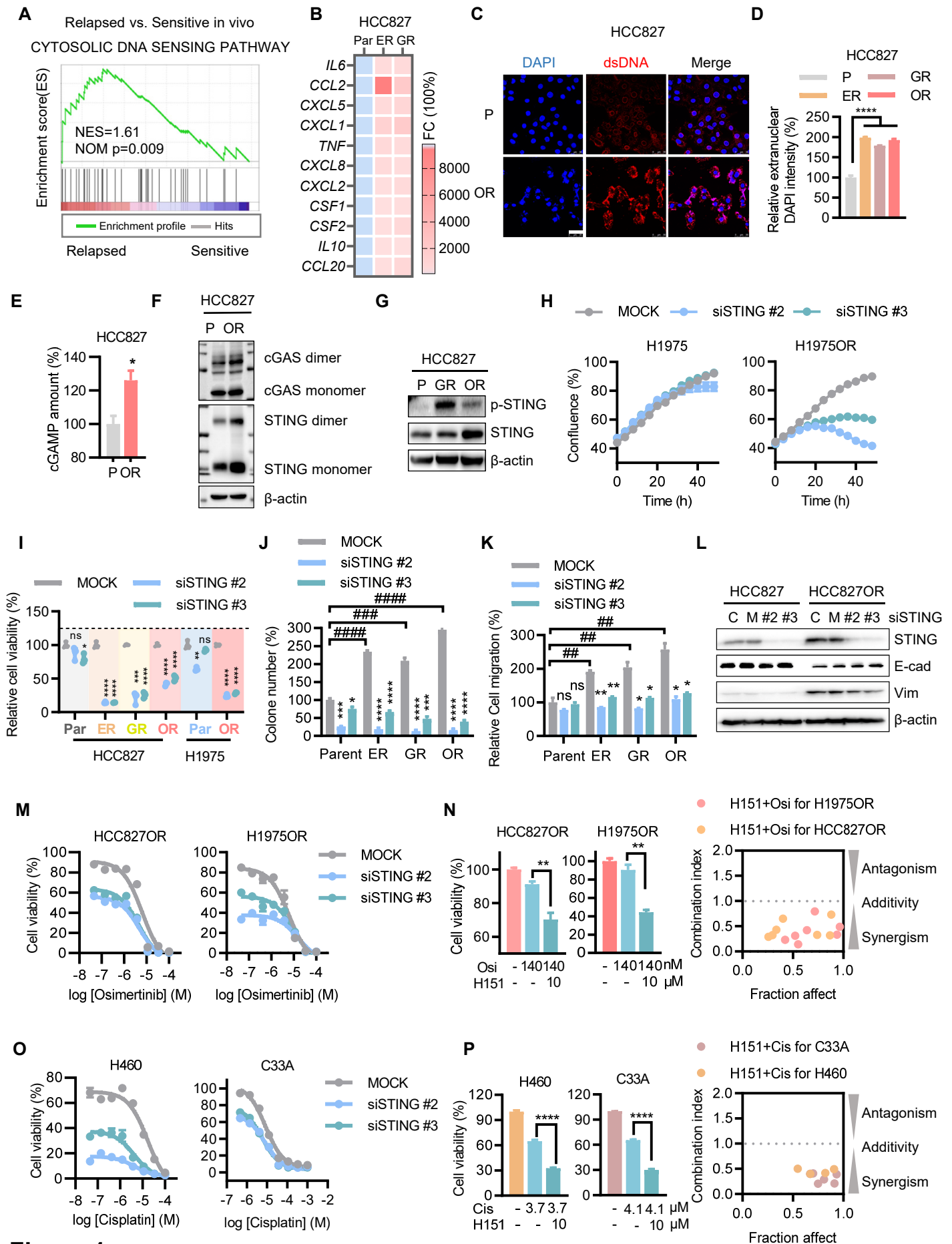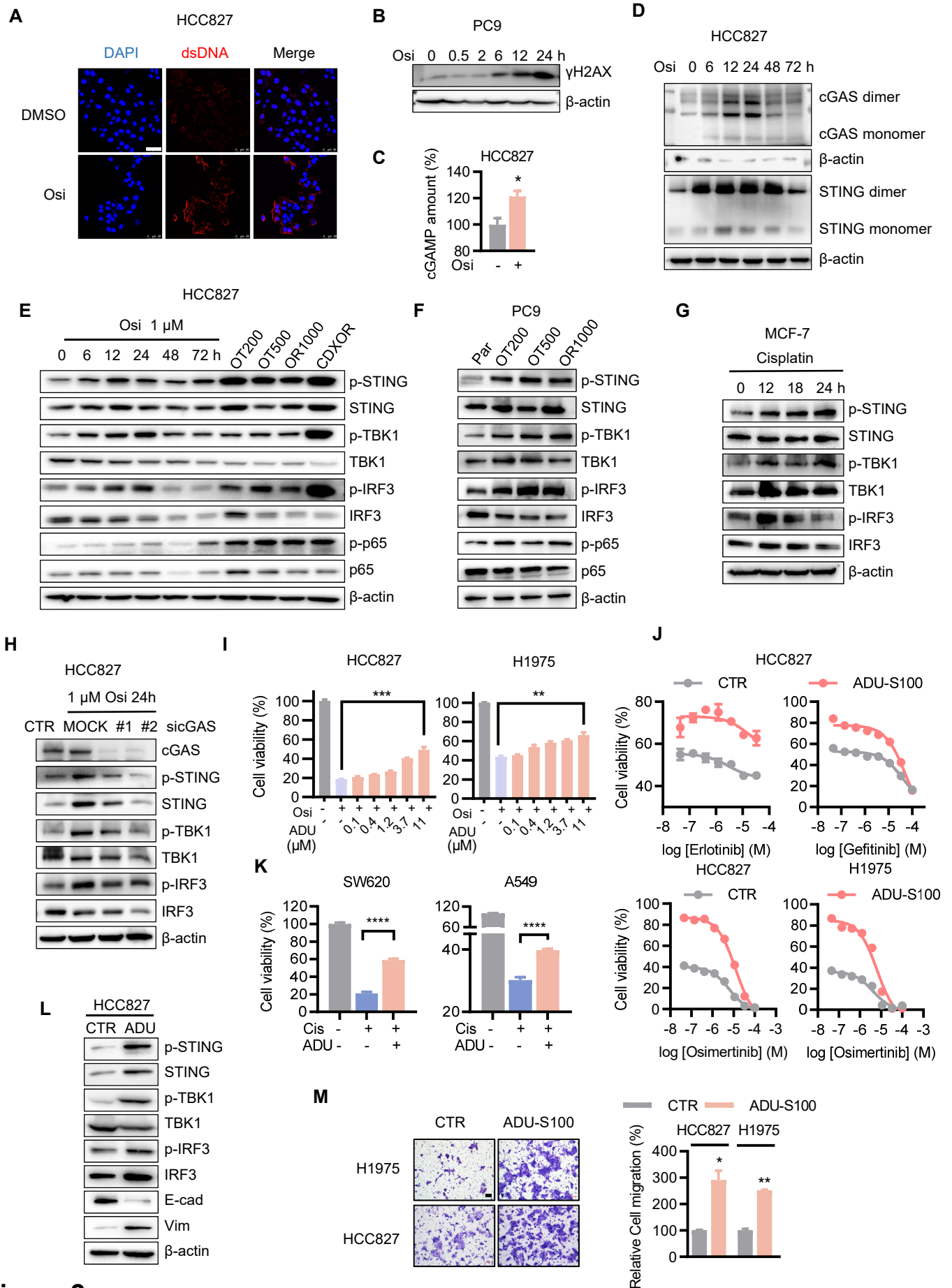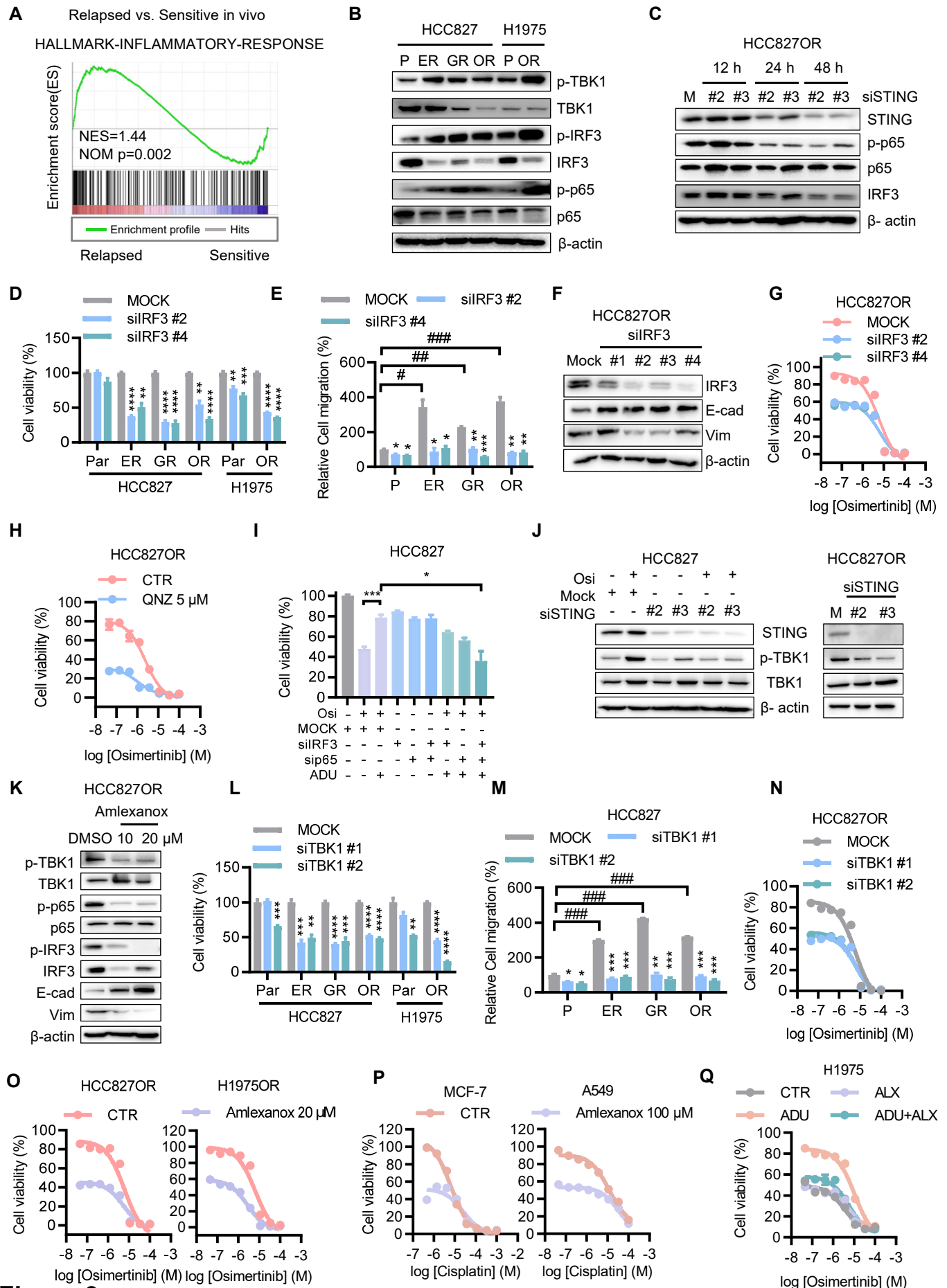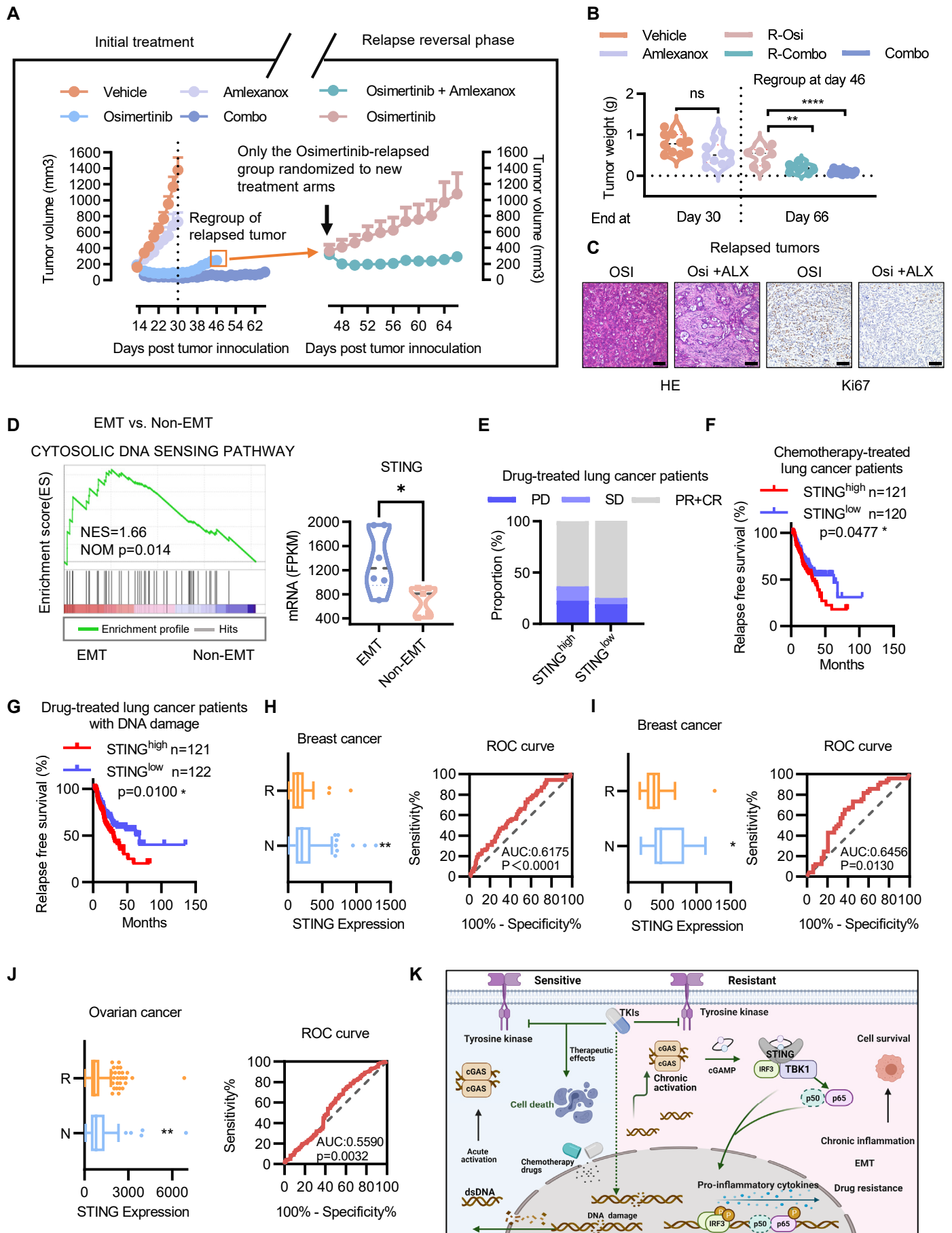
24

622   BioRender.com.

Figure 1.

Figure 2.

Figure 3.

Figure 4.